Geochemistry Geophysics Geosystems G3

Article
Volume 13, Number 1
18 February 2012
Q0AK04, doi:10.1029/2011GC003818
ISSN: 1525-2027

Published by AGU and the Geochemical Society

Upper mantle *P* velocity structure beneath the Midwestern United States derived from triplicated waveforms

Risheng Chu, Brandon Schmandt, and Don V. Helmberger

Seismological Laboratory, California Institute of Technology, Pasadena, California 91125, USA (chur@gps.caltech.edu)

[1] Upper mantle seismic velocity structures in both vertical and horizontal directions are key to understanding the structure and mechanics of tectonic plates. Recent deployment of the USArray Transportable Array (TA) in the Midwestern United States provides an extraordinary regional earthquake data set to investigate such velocity structure beneath the stable North American craton. In this paper, we choose an M_w5.1 Canadian earthquake in the Quebec area, which is recorded by about 400 TA stations, to examine the *P* wave structures between the depths of 150 km to 800 km. Three smaller Midwestern earthquakes at closer distance to the TA are used to investigate vertical and horizontal variations in *P* velocity between depths of 40 km to 150 km. We use a grid-search approach to find the best 1-D model, starting with the previously developed S25 regional model. The results support the existence of an 8° discontinuity in *P* arrivals caused by a negative velocity gradient in the lithosphere between depths of 40 km to 120 km followed by a small (∼1%) jump and then a positive gradient down to 165 km. The *P* velocity then decreases by 2% from 165 km to 200 km, and we define this zone as the regional lithosphere-asthenosphere boundary (LAB). Beneath northern profiles, waves reflected from the 410 discontinuity (410) are delayed by up to 1 s relative to those turning just below the 410, which we explain by an anomaly just above the discontinuity with *P* velocity reduced by ∼3%. The 660 discontinuity (660) appears to be composed of two smaller velocity steps with a separation of 16 km. The inferred low-velocity anomaly above 410 may indicate high water concentrations in the transition zone, and the complexity of the 660 may be related to Farallon slab segments that have yet to sink into the deep mantle.

Components: 9300 words, 14 figures, 1 table.

Keywords: North American craton; lithosphere-asthenosphere boundary; low-velocity zone; transition zone; upper mantle structure.

Index Terms: 7208 Seismology: Mantle (1212, 1213, 8124); 7218 Seismology: Lithosphere (1236); 8103 Tectonophysics: Continental cratons.

Received 28 July 2011; **Revised** 11 January 2012; **Accepted** 11 January 2012; **Published** 18 February 2012.

Chu, R., B. Schmandt, and D. V. Helmberger (2012), Upper mantle *P* velocity structure beneath the Midwestern United States derived from triplicated waveforms, *Geochem. Geophys. Geosyst.*, *13*, Q0AK04, doi:10.1029/2011GC003818.

Theme: The Lithosphere-Asthenosphere Boundary

1. Introduction

[2] Upper mantle seismic velocity structure and its variations in both vertical and horizontal directions provide key information about plate dynamics and the role of the "tectosphere" that underlies stable Precambrian cratons [*Jordan*, 1978]. Jordan argues that thick continental lithosphere is neutrally buoyant on account of a balance between increased buoyancy from iron depletion and decreased buoyancy from cold temperatures in a thick thermal boundary layer. The subsequent accumulation of research on the structure and evolution of continental lithosphere finds much merit in this tectosphere hypothesis, but also growing evidence that the stability of thick continental lithosphere is not universal [*Carlson et al.*, 2005; *Lee et al.*, 2011]. Removal of continental lithosphere has been suggested beneath the Wyoming and north China Archean cratons [*Carlson and Irving*, 1994; *Gao et al.*, 2002] and beneath Proterozoic provinces of the southwestern Great Plains [*Song and Helmberger*, 2007] and Colorado Plateau [*Bird*, 1979; *Levander et al.*, 2011]. Resolving detailed *P* and *S* velocity structure beneath additional cratonic regions will better illuminate the prevalence of lithospheric instabilities beneath continental interiors and the physical and chemical characteristics of intact Precambrian lithosphere. Recently acquired USArray Transportable Array (TA) data provides a new opportunity to survey upper mantle structure beneath a large portion of the North America's stable Precambrian interior.

[3] Further insight into mantle processes active beneath the continental lithosphere as well as the nature of the transition zone between the upper and lower mantle can be gained by determination of seismic velocity structure between depths of ~300–700 km. Discontinuities near 410 km and 660 km depth formally delimit the mantle transition zone and are thought to primarily reflect phase transitions of olivine with increasing pressure and temperature [*Ringwood*, 1975]. Seismic observations suggest a second discontinuity near 660 km depth exists in some regions [*Simmons and Gurrola*, 2000; *Ai et al.*, 2003; *Deuss et al.*, 2006] consistent with the majorite garnet to perovskite transition expected for a pyrolitic mantle [*Vacher et al.*, 1998]. In addition to constraints on bulk composition, upper mantle velocity structure may also provide constraints on mantle water concentration. The presence of low-velocity layers atop the 410 km discontinuity is potentially a sign of high water concentrations in the transition zone [e.g., *Bercovici and Karato*, 2003]. There are increasing reports that such low-velocity layers exist sporadically beneath North America [*Song and Helmberger*, 2006; *Gao et al.*, 2006; *Courtier and Revenaugh*, 2006; *Jasbinsek and Dueker*, 2007; *Schaeffer and Bostock*, 2010; *Schmandt et al.*, 2011] and globally [*Tauzin et al.*, 2010], but there are no previous investigations of its presence beneath the central U.S. The depths of olivine phase transitions, the relative importance of garnet phase transitions, and mantle water concentrations may all be altered by subduction of ocean lithosphere, which has been occurring beneath the western margin of North America for >150 Ma [*Engebretsen et al.*, 1985]. This history of subduction is suggested to influence upper mantle discontinuity structure beneath the western U.S. [*Cao and Levander*, 2010; *Eagar et al.*, 2010; *Schmandt et al.*, 2011] and part of the central U.S. [*Li et al.*, 1998]. Influence of subduction on upper mantle structure far beneath the continental interior may be expected on account of low-angle subduction during the Laramide orogeny [*Coney and Reynolds*, 1977; *Liu et al.*, 2008].

[4] Various teleseismic imaging methods have been applied to TA data to map upper mantle seismic structure. Body wave travel-time tomography [*Burdick et al.*, 2009; *Sigloch et al.*, 2008; *Roth et al.*, 2008; *Obrebski et al.*, 2010; *Schmandt and Humphreys*, 2010] and surface wave dispersion tomography [*Moschetti et al.*, 2010; *Pollitz and Snoke*, 2010], and receiver function analysis [*Cao and Levander*, 2010] are among the most frequently applied methods. Model variability from body wave travel-time inversions appears quite high [e.g., *Sun and Helmberger*, 2011]. While these inversions can explain well travel-time residuals for teleseismic phases, their use of global 1-D reference models typically renders them inconsistent with measurements of phases that are sensitive to regional 1-D structure (e.g., upper mantle triplications). Indeed, synthetic waveforms produced by such models are found to provide poor fits to regional *P* waveforms for phases that travel horizontally in the upper mantle [*Chu et al.*, 2012]. Replacing the commonly used AK135 reference model [*Kennett et al.*, 1995] with mT7 (Figure 1) is shown to greatly improve regional waveform fits [*Chu et al.*, 2012].

[5] Modeling of the differential waveforms such as *SS-S*, or pure-path regional modeling, can help alleviate source uncertainty issues and improve vertical resolution of regional 1-D velocity structure [*Grand and Helmberger*, 1984] and consequently

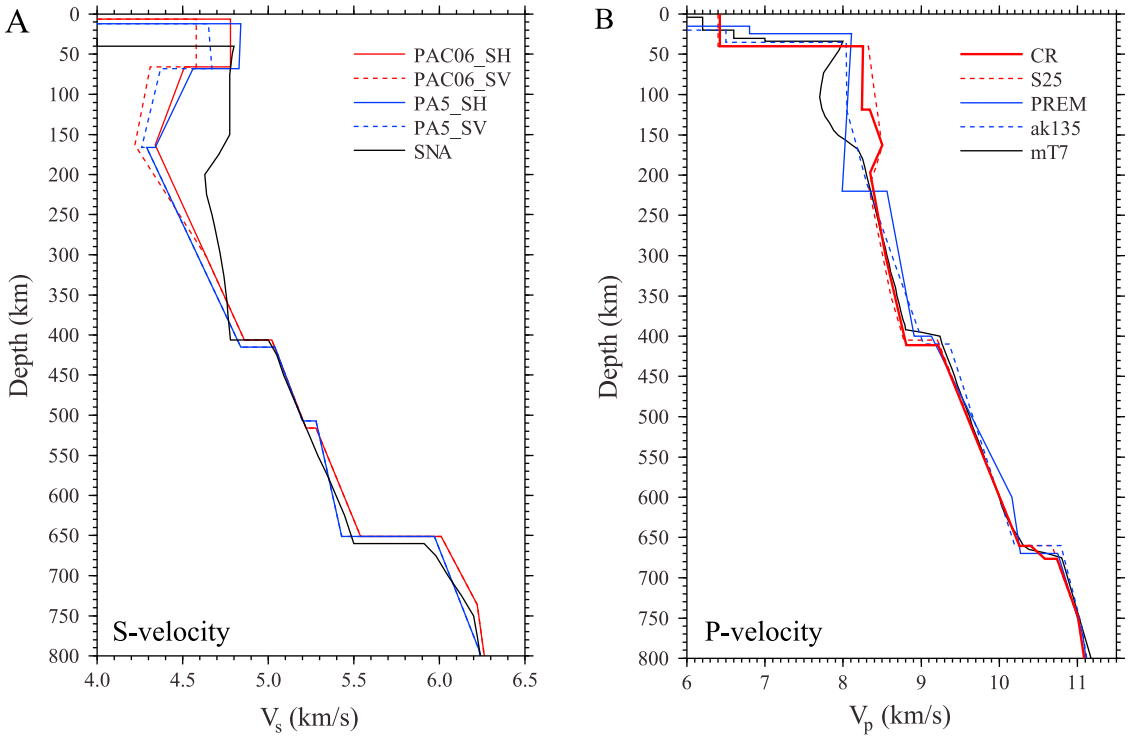

Figure 1. Proposed upper mantle models with (left) *S* velocities and (right) *P* velocities. (a) Comparison of *S* velocity models for the Pacific Basin, PAC06 [*Tan and Helmberger*, 2007] and PA5 [*Gaherty et al.*, 1996], and the North America shield [*Grand and Helmberger*, 1984]. (b) Comparison of *P* velocity models for the North American craton (CR), the Canadian Shields (S25) [*LeFevre and Helmberger*, 1989], global average model PREM [*Dziewonski and Anderson*, 1981] and AK135 [*Kennett et al.*, 1995], and the Basin and Range (mT7) [*Chu and Helmberger*, 2011].

allow improved comparison of different tectonic regions. Examples of Pacific Basin shear-velocity models are displayed in Figure 1a, with a 1D model PAC06 determined by modeling multibounce *S* waves using a grid-search method to fully investigate interdependencies among model parameters [*Tan and Helmberger*, 2007]. Another velocity model, PA5, is determined by complete seismogram inversion [*Gaherty et al.*, 1996]. The $V_{SH} > V_{SV}$ transverse anisotropy appears compatible among these models as well as those reported by *Ekström and Dziewonski* [1998] and is expected for oceanic upper mantle structure produced by plate spreading [*Zhang and Karato*, 1995]. Radial anisotropy with $V_{SH} > V_{SV}$ is also reported beneath stable continental regions [*Godey et al.*, 2004; *Matzel and Grand*, 2004; *Nettles and Dziewonski*, 2008; *Yuan and Romanowicz*, 2010], although beneath stable parts of continents the maximum radial anisotropy is found within the high-velocity lid whereas in oceanic regions it tends to occur in the low-velocity zone [*Nettles and Dziewonski*, 2008]. Another difference between oceanic and continental regions is that the *S* velocity gradient between 200 and 400 km depth in Pacific models is much steeper than that beneath the North American craton (i.e., SNA) [*Grand and Helmberger*, 1984]. *Gaherty et al.* [1999] argue that such features could reflective convective processes beneath oceanic plates, which differs from stable continental interiors where a thicker conductive boundary is thought to exist. Other hypotheses, including changing grain size with depth [*Faul and Jackson*, 2005], transition from pure dislocation to diffusion creep with depth [*Karato and Wu*, 1993], and variations in pyroxenite contribution to velocity structure with depth [*Stixrude and Lithgow-Bertelloni*, 2005] have also been proposed to explain this steeper velocity gradient. A corresponding *P* velocity structure would help address the causes of the vertical velocity gradient as well as understanding of the structural contrasts between the lithosphere-asthenosphere boundary in oceanic and continental regions. A recent review by *Fischer et al.* [2010] provides an up-to-date perspective on the lithosphere-asthenosphere boundary beneath oceanic plates, stable cratons, and tectonically active continental regions.

[6] To demonstrate the profound variations between global and regional 1-D models we display several

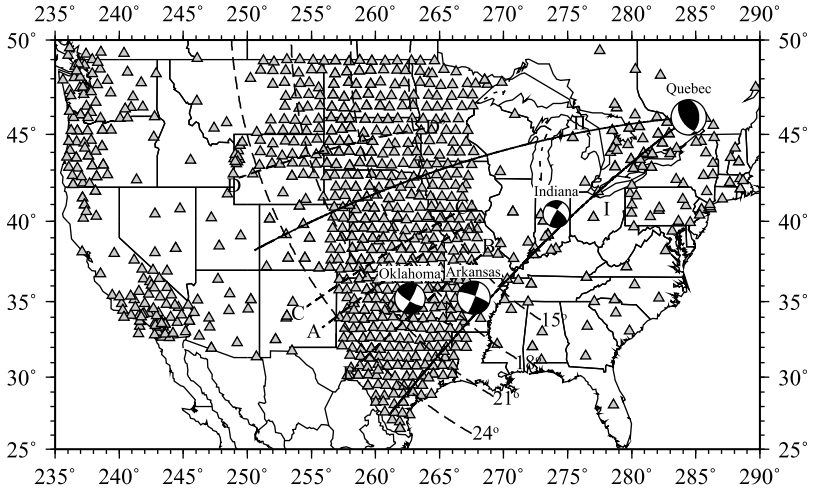

Figure 2. Map of the United States displaying the locations of earthquakes and broadband seismic stations used in this study. Beach balls represent focal mechanism obtained using the CAP method with source information given in Table 1. The Quebec earthquake provides the triplication data with three profiles of data at ranges 15° to about 25° indicated by dotted lines. Detailed observations will be presented along sub-corridors, AA′–DD′, and stacks bracketed by I and II discussed later in the text.

commonly used *P* velocity models in Figure 1b along with the recently introduced mT7 model for western United States [*Chu and Helmberger*, 2011]. A relatively old regional model for stable North America, S25, is derived from a combination of travel-time data from large Early Rise explosions fired in the Great Lakes [*Mereu and Hunter*, 1969] and *PP-P* bounce data from the same events used to derive SNA [*Grand and Helmberger*, 1984]. The latter study uses hand digitized analog data from old Air Force linear arrays, long-range seismic measurements (LRSM). An important advantage of such studies is that the explosions have known locations and origin times, although the disadvantage is the lack of station coverage. Even with sparse station coverage by today's standards, it is clear that the Gnome explosion in eastern New Mexico produces distinctly different record sections for waves propagating east and west from the source [*Romney et al.*, 1962]. The two models mT7 (West) and S25 (East) roughly explain the reported travel time differences and many characteristics of the waveforms recorded by the TA for recent earthquakes near the Rocky Mountain Front tectonic boundary. The preferred 1-D model resulting from this study, CR, has many similarities with S25. The most prominent differences between CR and S25 are a more complicated lithosphere and a double discontinuity near 660 km that comprises the boundary with the lower mantle.

[7] The objective of this study is to introduce a 1-D reference *P* velocity model for the upper mantle beneath the stable region of North America by modeling waveforms of regional earthquakes recorded by the TA. First, we address the source properties of the small earthquakes used in this study. We then briefly review the triplications predicted by three reference models (PREM, AK135, and S25), and compare them to a stacked record section of waveforms from the Quebec event ($M_w = 5.1$) recorded by the TA. This comparison is followed by detailed presentation of results from forward modeling of triplication data with 1-D velocity models using a grid-search method. A separate section is devoted to lithospheric structure constrained by the modeling of shallow upper mantle phases produced by three other earthquakes that occurred at closer distances to most TA stations (<15°). In the final section we discuss implications of the new regional 1-D *P* velocity model for continental structure, physical and chemical properties of the mantle transition, and the history of subduction beneath North America.

2. Earthquake Data

[8] Large explosions are particularly useful for studying the 1D *P* velocity structure because of their relatively simple waveforms as exploited by many researchers [e.g., *Given and Helmberger*, 1980]. Although small explosions are still popular in crustal studies, large explosions are less common nowadays. Therefore we have to rely on the relatively low seismicity of the stable craton and exploit the dense wide-aperture receiver coverage provided by the TA (Figure 2). In this study, we

Table 1. Earthquake Used in This Study

ID	Origin Time	Latitude	Longitude	H (km)	M_w	Strike/Dip/Rake (deg)	Source
Quebec	2010/06/23, 17:41:42.6	45.95	284.45	19.0	5.0	162/46/88	NEIC[a]
	2010/06/23, 17:41:41.0	45.90	284.50	16.4	5.0	NA	NRCAN[b]
	2010/06/23, 17:41:42.0	45.86	284.54	22.0	5.0	145/60/80	SLU[c]
	2010/06/23, 17:41:46.0	45.97	284.42	22.7	5.0	152/49/82	GCMT
	NA	NA	NA	19.0	5.0	146/55/68	CAP[d]
	NA	NA	NA	19.0	5.1	151/48/84	CAPt[e]
Oklahoma	2010/10/13, 14:06:29.5	35.21	262.69	14.0	4.3	120/80/5	SLU
	NA	NA	NA	12.0	4.3	121/76/7	CAP
Indiana	2010/12/30, 12:55:21.0	40.43	274.11	14.0	3.8	305/65/10	SLU
Arkansas	2011/02/28, 05:00:50.2	35.26	267.66	4.0	4.7	295/80/−5	SLU
	NA	NA	NA	4.0	4.7	297/84/7	CAP

[a]United States Geological Survey National Earthquake Information Center, last accessed on June 24, 2010.
[b]Natural Resources Canada.
[c]From http://www.eas.slu.edu/Earthquake Center/MECH.NA, last accessed March 3, 2011. See *Herrmann et al.* [2011] for more details.
[d]The velocity model used here is modified from *Herrmann* [1979].
[e]At the frequency range of 0.02 to 1.0 Hz, we cut the waveform using a time window of 13 s. See Chu et al. (submitted manuscript, 2011) for more details.

select four earthquakes located in and around the North American craton. Among them, the Quebec earthquake is the most important because its 15°–25° raypaths provide nearly complete radial sampling of upper mantle velocity structure (Figure 2).

[9] Before we can study the *P* wave propagations of these earthquakes, we need to determine their source parameters. Various focal-mechanism solutions have been provided by different organizations (Table 1) along with our regional mechanism that employs the Cut-and-Paste (CAP) method (Figures S1–S3 in the auxiliary material).[1] This technique fits P_{nl} and surface wave segments between observed and synthetics that are allowed to shift independently in timing for alignment [*Zhu and Helmberger*, 1996]. Thus, the procedure automatically determines the travel-time delays along each path. This particular event is difficult to locate with *P* wave travel times because of the nodal first P_n arrivals at local stations. Regional Rayleigh waves at period of 10 s have proven useful in locating earthquakes as discussed by *Tan et al.* [2010]. Thus, we search for a location that has similar delays in all azimuths and found the SLU location to be preferable. In Figure 3a, we display the Rayleigh wave delays using the SLU location.

[10] We also invert the focal mechanism of the Quebec earthquake using a teleseismic version (CAPt) (R. Chu et al., Inversion of source parameters for moderate earthquakes using short-period teleseismic *P* waves, submitted to *Geophysical Journal International*, 2011), obtaining a slightly different solution (Figure 3a and Table 1). In Figure 3b, we include the fits of synthetic waveforms of teleseismic data observed in western United States for the Quebec earthquake whose azimuths sample the TA stations. Both *P* and *pP* are relatively weak on the waveforms. The strongest phase is the depth phase *sP* which is well separated from *P*. Such source complexity, unfortunately, must be accepted since it is the only event available in the region. Note that the *sP* phase is commonly observed in this region for small earthquakes and has been successfully used in double-difference relocations [*Ma and Eaton*, 2011].

3. Stacking of Triplicated Waveforms

[11] At regional distances between 10° and 30°, waveforms of the Quebec earthquake are complicated by upper mantle triplications, which result from discontinuities near 410 km and 660 km. Before presentation of the regional *P* wave record sections, we review the triplications generated from three reference models for a simple impulsive explosion-type source (Figure 4). To generate synthetics, we employ a variety of methods including generalized ray theory (GRT), standard frequency wave number integration, WKM (a generalization of WKB), and finite difference codes. See *Chu et al.* [2012] for applications similar to this study. In Figure 4, the GRT technique is applied to three reference models (PREM, AK135, S25), which produce distinctly different upper mantle raypaths. Perhaps the most obvious difference between the reference models is that the 220 km discontinuity unique to PREM produces an extra triplication, with particularly strong arrivals for distances

[1]Auxiliary materials are available in the HTML. doi:10.1029/2011GC003818.

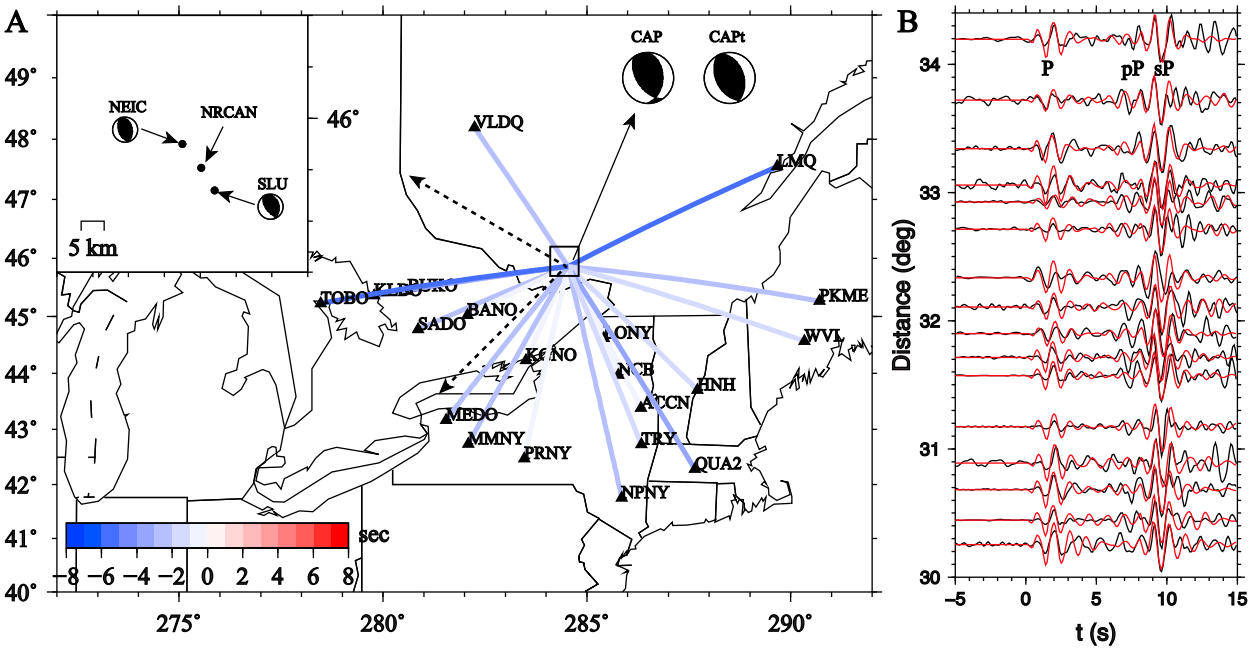

Figure 3. Source parameters derived for the Quebec earthquake. (a) The stations used in the regional Cut-and-Paste (CAP) inversion are given as triangles in the map view. The inset shows locations and mechanisms from different organizations (Table 1). Our focal mechanism derived by modeling the regional and teleseismic waveforms are compared to those in the inset. Regional Rayleigh-wave travel-time residuals (paths with travel-time delays) from the regional inversion favor the SLU location. The two beach balls are focal mechanisms inverted using regional (CAP) and teleseismic (CAPt) waveforms. (b) Comparison of observed velocity in the vertical direction (black) and synthetics (red) recorded by stations on the west coast. These observations are recorded at azimuths enclosed by the dashed vectors in Figure 3a, essentially from south to north. Direct *P* and the depth phases, *pP* and *sP*, are labeled on the bottom. Both data and synthetics are filtered at frequency band of 0.8–2.0 Hz and align on the direct *P*. Unfortunately, the direct *P* and *pP* become nodal at triplication distance but *sP* remains strong.

beyond 25° and reduced times greater than 50 s. Model S25 has a late arriving AB branch at large distances and displays an offset near 19° caused by its low-velocity zone starting at 170 km depth. This branch is observed for cratons in several regions as discussed by *LeFevre and Helmberger* [1989].

[12] A convolution with the radiation pattern of the Quebec earthquake produces a complex profile with a rather weak direct *P* and *pP* followed by a strong *sP* arrival (Figure 5). The nodal characteristics of direct *P* make it difficult to decipher the *P* branches but the CD branch of *sP* is readily identified. We add a reference line to help compare the synthetics with the observed CD branch. In Figure 5b, we include three cross-sections sampling several azimuths. The station coverage is not uniform as a result of the source-array geometry (Figure 2). Nevertheless, the CD and AB branches of *sP* are apparent, especially at the larger ranges. These features become clearer when the data are stacked.

[13] To improve stack coherence, we take some liberty in making some small timing adjustments to correct for local structure. This is done by cross-correlating S25 synthetics with individual records, and allowing small shifts in timing so phase slownesses that are representative of the 1-D velocity structure near ray turning depths can be better identified. Examples of records requiring time shifts for local structure are presented in Figure 6. At the nearest distances (∼15°), sP_{AB} is slightly early or late (M35A–V37A in Figure 6), but because the sP_{CD} branch is stronger, it is used to control the alignment. At greater distances (∼18–20°, Y39A–S28A in Figure 6), the AB and CD arrivals interfere as the extended AB branch is bottoming below the LAB. The S25 predictions require some local timing adjustments, which are, again, controlled by the stronger sP_{CD} arrival. At distances beyond 22°, the time separation between sP_{CD} and sP_{AB} is greater and the cross-correlation coefficients (CCs) between synthetic and observed waveforms increase. This character of improved waveform fit with increasing distance is apparent in Figure 6b, where waveforms from most stations have CCs greater than 85%. The delays for all TA

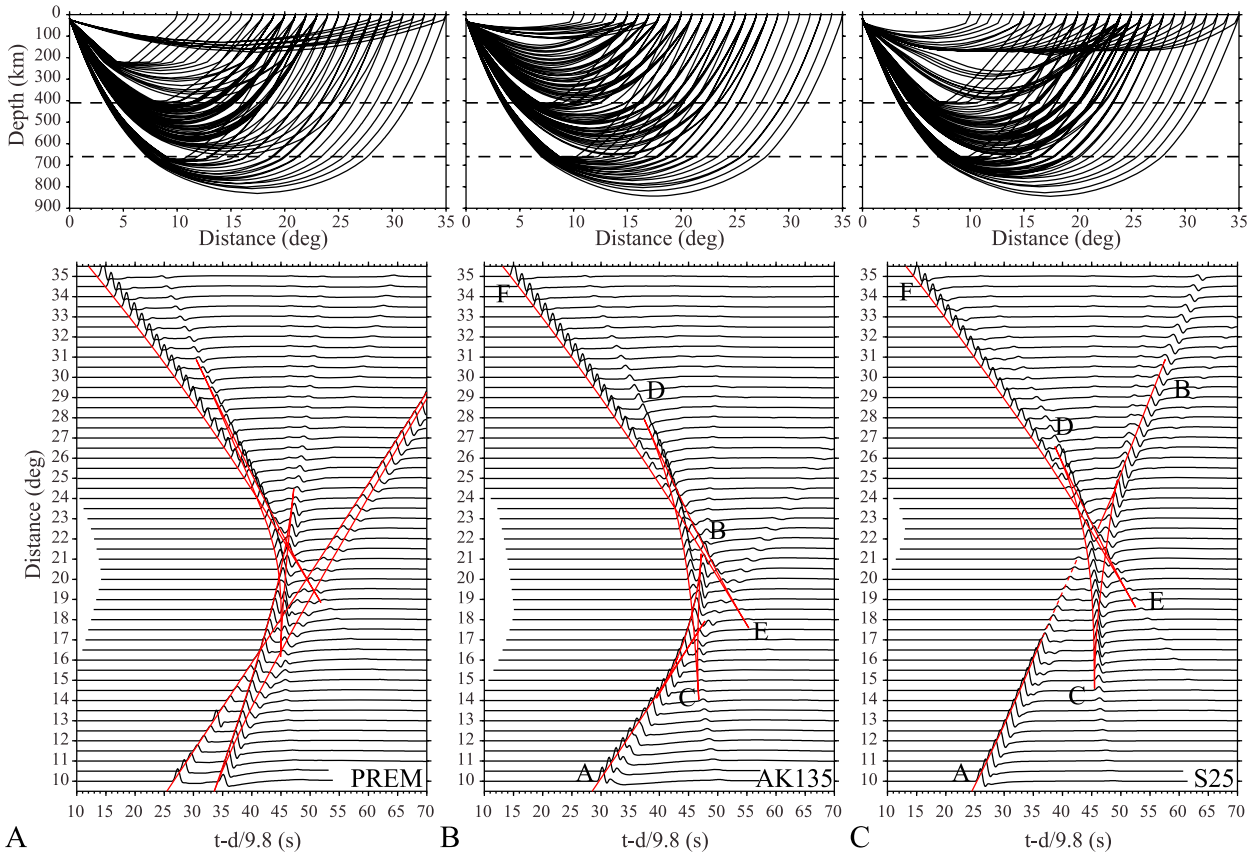

Figure 4. Raypaths and synthetics for velocity model (a) PREM, (b) AK135, and (c) S25. Triplicated arrival times are displayed in red lines. Seismic rays travel above the 410 discontinuity, in the transition zone, and below the 660 discontinuity are referred to as AB, CD, and EF branch, respectively. The heavy dotted lines indicate the positions of the major transition discontinuities. Due to the LAB of S25 between 165 and 210 km, the AB branch has an offset at the distance of 19° and 21°, and can be seen at distance larger than 27°. An extra triplication for PREM is observed because of the discontinuity at 220 km, which is not observed and not labeled.

stations and their cross-correlation values are shown in Figure 6b. There are a few stations with very low CCs but excluding them does not lead to a different optimal model so all stations are included in this analysis. Noteworthy is a zone of relatively slow arrivals near the South Dakota and Nebraska border that will be addressed in section 6 (Figure 6b).

[14] The stacked data along with synthetic waveforms for the best fitting model (CR) are presented in Figure 7, excluding the nearly nodal phases *P* and *pP*. A complete comparison is given in Figure S4. Remarkably, even this small event produces a detailed image of the *sP* phase triplications. Weaker and mostly nodal *P* and *pP* phases are also present, but less obvious. The sP_{AB} branch is clear at distances less than 18°, but at slightly greater distances the shadow zone (low-velocity zone) starting near the depth of 165 km reduces its strength. Increased amplitude of the sP_{AB} branch occurs beyond 22° where its raypaths turn below the low-velocity zone. The sP_{CD} branch dominates the triplication associated with the 660 discontinuity. This observation can be explained by the presence of two closely spaced jumps in velocity rather than the single jump present in global reference models (see section 4). Note that sP_{EF} appears at about 19° and only becomes the apparent first arrival beyond 25°. Unfortunately, at about this range, we are reaching the tectonic western province and the western extent of the TA stations at the time of this event. In the next section, we will discuss in detail how the CR model was constructed and present evidence for lateral variations near the 410 discontinuity.

4. Waveform Modeling of Triplications

[15] Although the upper mantle structure is a complex 3-D structure, we will assume that the triplications involving the transition zone discontinuities

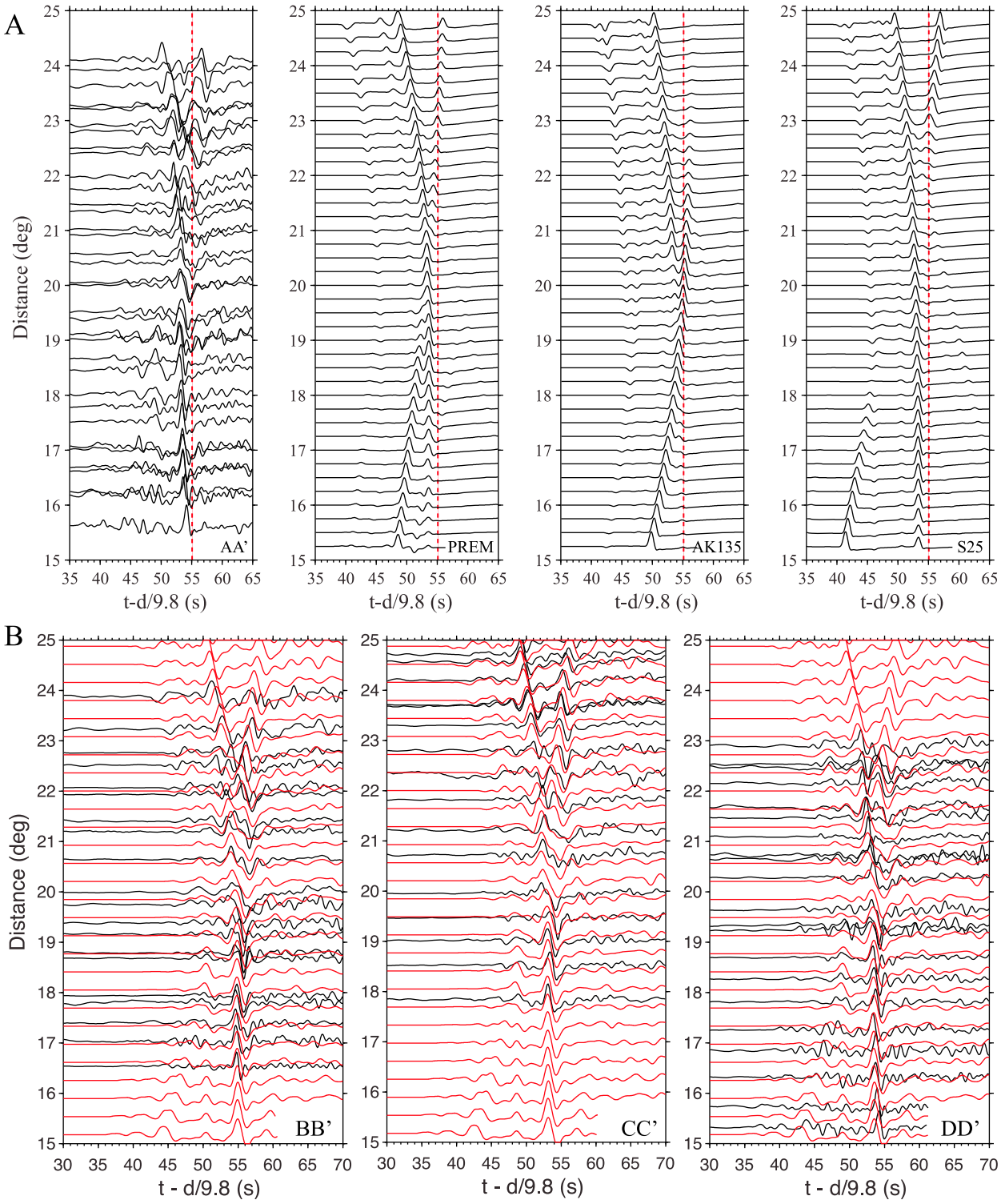

Figure 5. (a) Comparison of observed data and synthetics generated from velocity model PREM, AK135, and S25 for profile AA' indicated in Figure 2. Red dashed line is for reference only. It is obvious that model S25 fits the data better among the three models. (b) Comparison of vertical displacement (black) and finite difference synthetics (red) for profiles BB', CC', and DD' for velocity model S25. Both data and synthetics are filtered using a frequency band of 0.02–1.0 Hz.

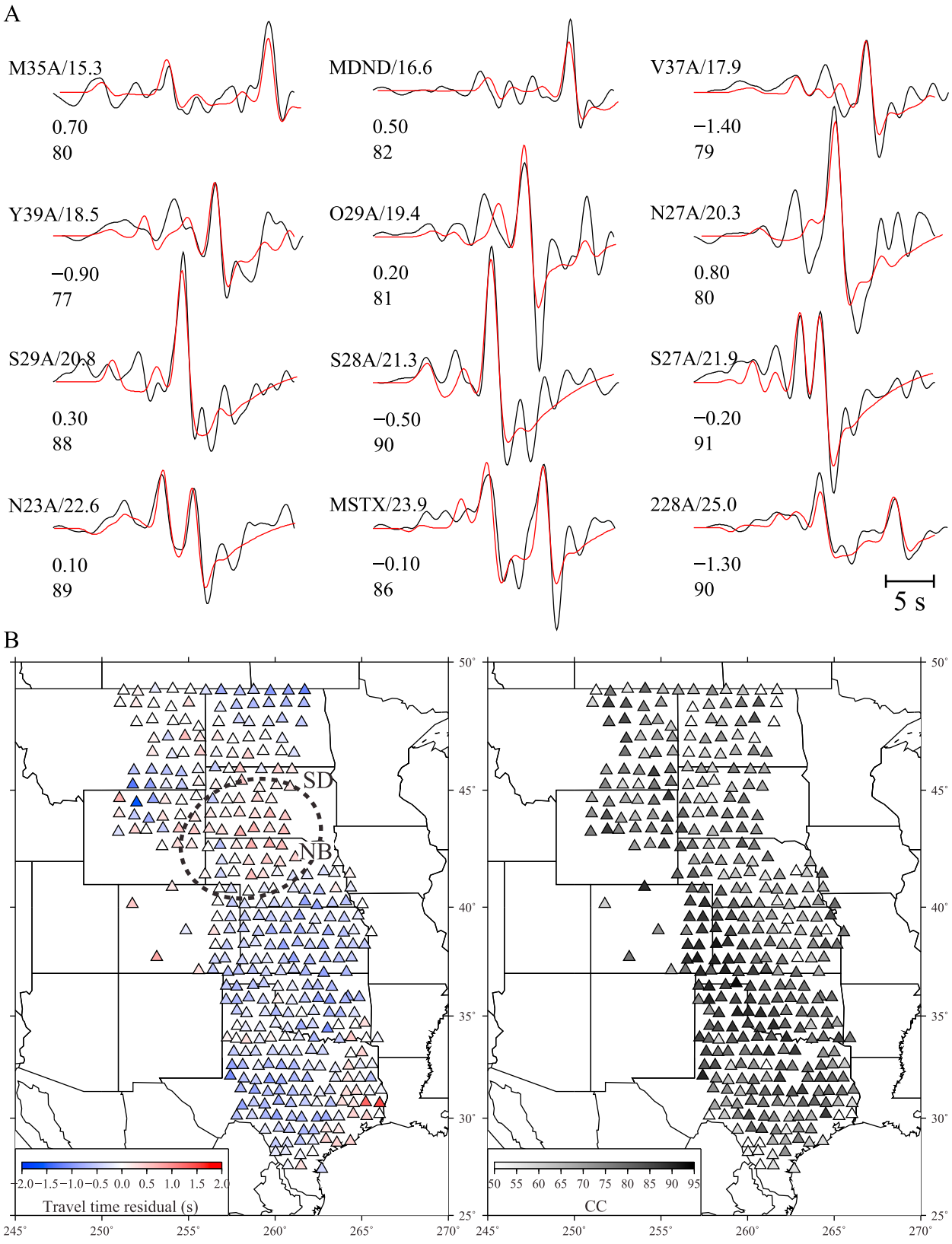
A
M35A/15.3
0.70
80
MDND/16.6
0.50
82
V37A/17.9
−1.40
79
Y39A/18.5
−0.90
77
O29A/19.4
0.20
81
N27A/20.3
0.80
80
S29A/20.8
0.30
88
S28A/21.3
−0.50
90
S27A/21.9
−0.20
91
N23A/22.6
0.10
89
MSTX/23.9
−0.10
86
228A/25.0
−1.30
90
5 s
B
SD
NB
−2.0 −1.5 −1.0 −0.5 0.0 0.5 1.0 1.5 2.0
Travel time residual (s)
50 55 60 65 70 75 80 85 90 95
CC
245° 250° 255° 260° 265° 270°
50° 45° 40° 35° 30° 25°

Figure 6

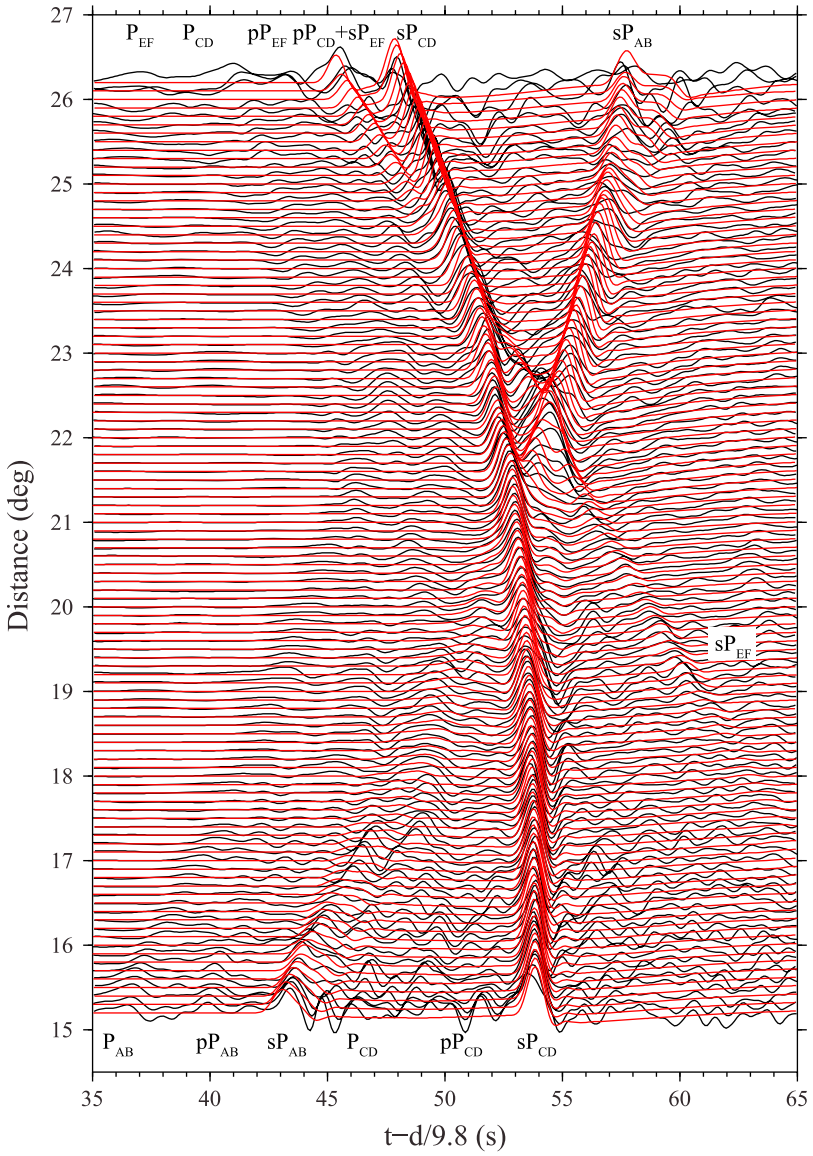

Figure 7. Comparison of stacked data (black) with synthetics (red) for the final model CR. In order to minimize the effect from the Texas coast and the Black Hills, the data for the southern stations between an azimuth of 230° and 265° (denoted by line I and II in Figure 2, respectively) is stacked using a bin size of 0.1°. Since *P* and *pP* are in the nodal direction, only *sP* is displayed in synthetics. Triplications of *P*, *pP*, and *sP* are labeled.

are dominantly 1-D in nature. Our basic approach is forward modeling through trial-and-error where we test models near S25 until we find one that fits the observed data. To reduce the number of parameters in the model construction, we have broken the model into mostly linear segments (Figure 8) where grid searches can be used to fine-tune the waveform fits, similar to the approach of *Tan and Helmberger* [2007]. We start from the top to minimize the trade-off between depth effects caused by shallow versus deep velocity variations.

[16] In Figures 8a and 8b, a collection of models are displayed for waveforms sampling the LAB region, which we define as the transition from the high-velocity lid to the upper mantle low-velocity zone.

Figure 6. (a) Examples of waveform fits for velocity model S25. The number after each station name is the epicentral distance in degrees. Two numbers below each trace are the time shifts with respect to the initial picking and cross-correlation coefficient (CCs). (b) Travel-time residuals and CCs across the whole TA for velocity model S25. The dashed oval represents the slow arrivals near the South Dakota (SD) and Nebraska (NB) border.

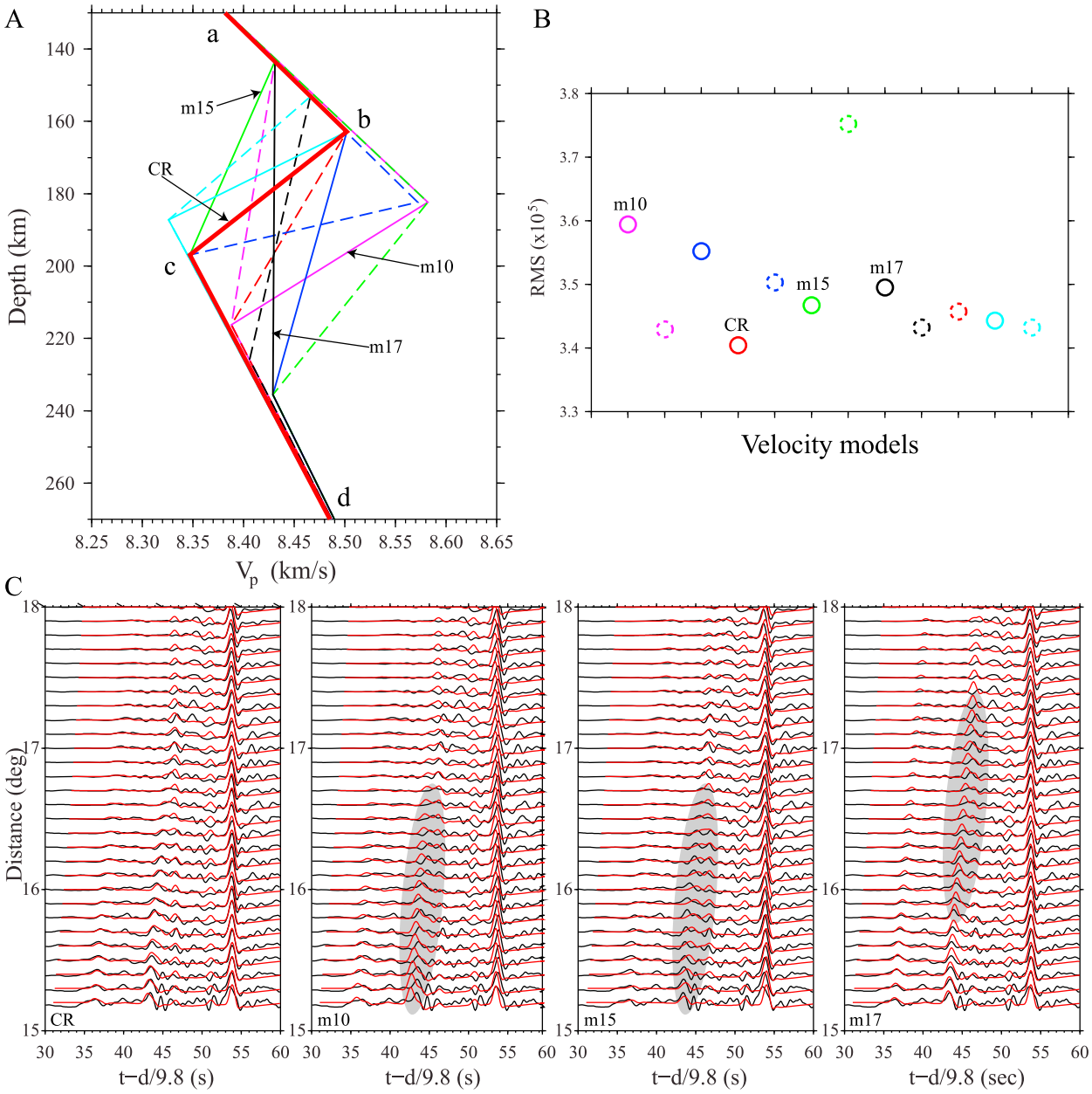

Figure 8. Grid search for the depth and thickness of the LAB. (a) Velocity models and (b) their root-mean square (RMS [*Zhu and Helmberger*, 1996]) are shown. The velocity models are color-coded for identification between A and B. (c) Waveform fits for our preferred model CR and three typical velocity models (m10, m15, and m17) are displayed. The m10 model has the largest separation between AB and CD branches; m15 has smaller AB amplitude, while the AB branch of m17 can be seen at about 18°, which are displayed in the shaded area.

The points b and c (Figure 8a) define the depth and value of the maximum lid velocity and the depth and value of the minimum of the low-velocity zone, respectively. To determine the optimal values of b and c we conduct a grid search in two directions, parallel and perpendicular to the S25 starting model. Moving the point b and c in the parallel direction will not change the slope of ab and cd, whereas moving b and c in the perpendicular direction changes the ab and cd slopes. Because the relative amplitude ratio of AB and CD branches is very sensitive to the slope of ab and cd (Figure S5), we fixed the slopes of ab and cd and grid-search the best positions of point b and c. This strategy determines the depth and sharpness of the LAB. In short, we generate synthetic waveforms for ~10 combinations of b and c to identify possible improvements to S25 starting model. However,

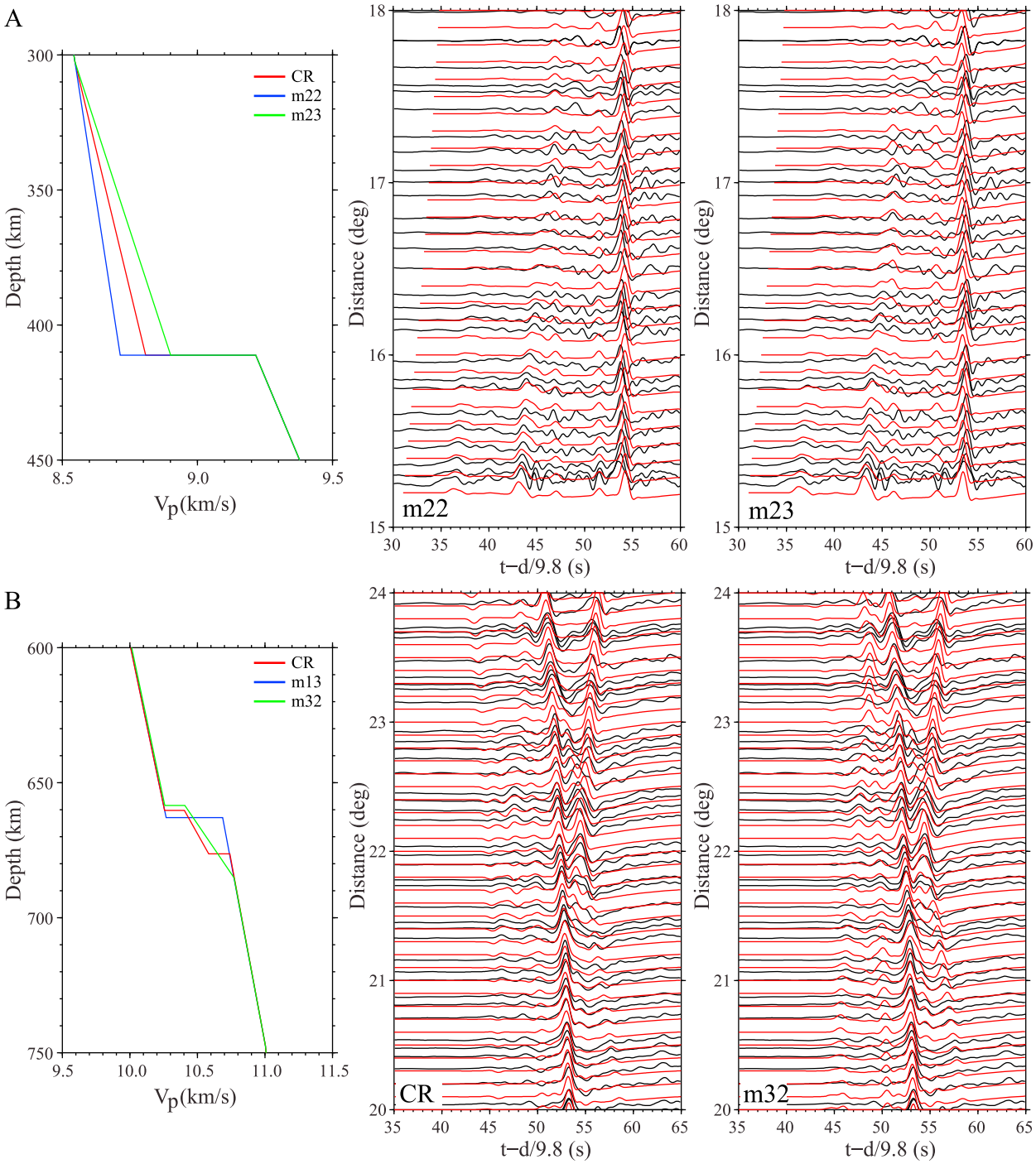

Figure 9. Display of some models tested for (a) the velocity-gradients above the 410 discontinuity and (b) sharpness of the 660 discontinuity. See Figures S5–S7 for more comparisons.

none of the fits are particularly good because interference from other phases involving *P* and *pP* make it difficult to define the extension of the AB branch into the shadow zone beyond 17° (Figure 8b). Thus, the CR model does not stand out even though the synthetic overlays for the CD branch compare well with the data. Waveform fits for our preferred model CR and three models with greater RMS are displayed in Figure 8c, with the shaded area highlighting poorly fit waveform segments.

[17] A similar search was conducted to investigate the structure of the 410 and 660 discontinuities, with example waveform fits shown in Figure 9. The

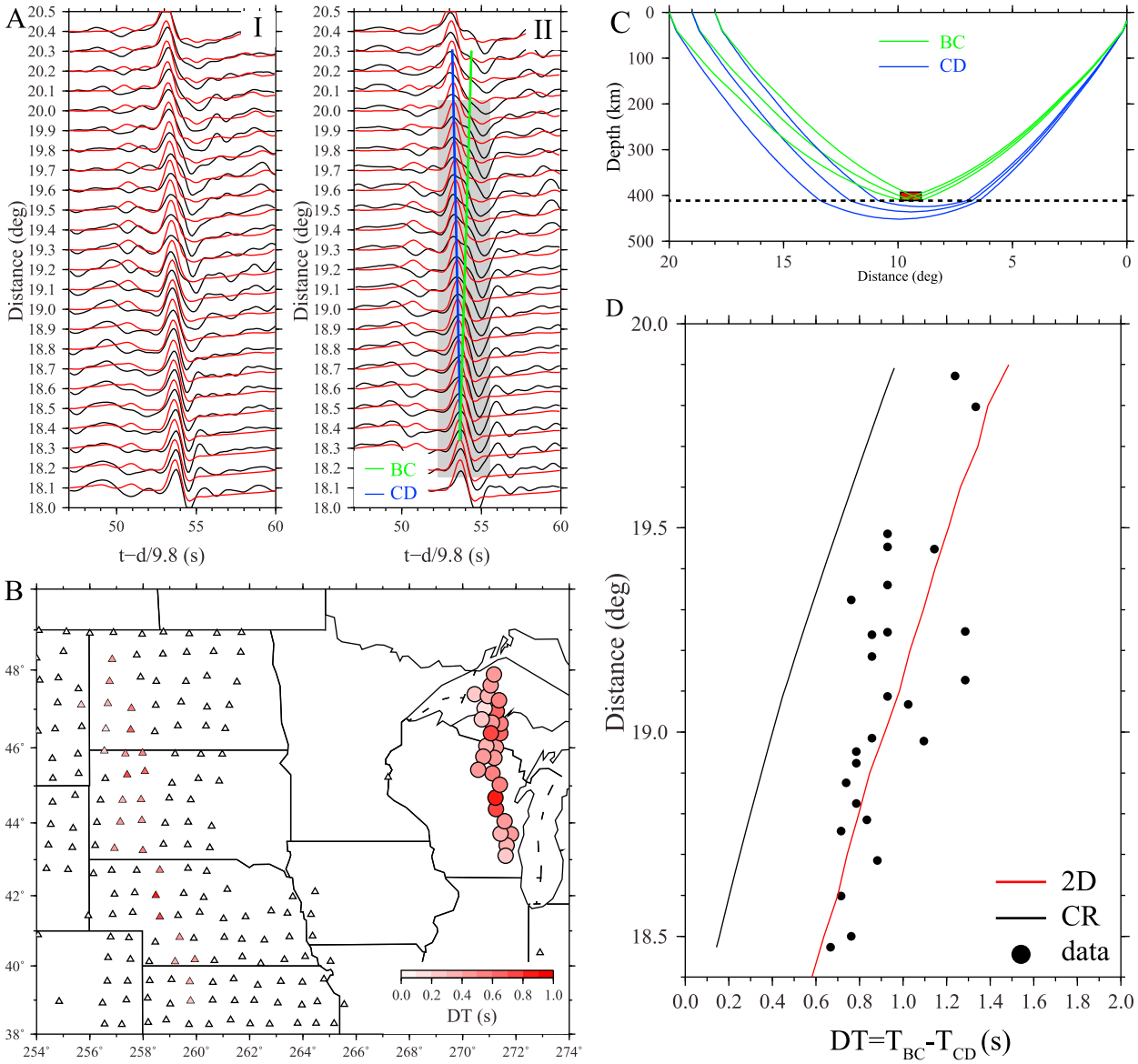

Figure 10. (a) Comparison of stacked data (black) and synthetics (red) for (left) the southern and (right) the northern stations between 18° and 20.5°. Note the broadened waveform for the northern stations, which is caused by larger CD-BC separations. The stations with larger CD-BC separations are displayed in (b) as color triangles. The colored circles represent the mid-points of anomalous paths. (c) Raypath for BC and CD branches at the distance of 18° to 20°. A low-velocity zone (LVZ) on the 410 discontinuity, denoted by the red box, will slow down the BC branch. Therefore the CD-BC separation will be larger. The LVZ, *P* velocity reduced by 3%, has a thickness of 20 km and a width of about 100 km. (d) Observed T_{CD}-T_{BC} (black dots) from individual records along with the predictions (red line) match reasonably well, although the scatter probably means variation in thickness or degree of possible melt. The black line denotes the T_{CD}-T_{BC} for 1D model CR.

most striking result is that a 660 discontinuity composed of two smaller jumps in velocity separated by 16 km fits the observed waveforms much better than the single larger jump in velocity from the S25 model. The primary reason for the double arrival is that the timing of the observed P_{EF} branch at the range 19° to 21° is not in agreement with the 22° to 23.5° branch for a single 660 jump. Thus, the initiation of the EF branch samples the upper boundary, but at larger ranges the deeper boundary dominates and explains the small offset in timing. Velocity models with broad gradients or single velocity jumps near 660 consistently provide poor fits to the data (Figure S6). It is possible that lateral variations in velocity structure could also produce the observed timing of the EF branch. However,

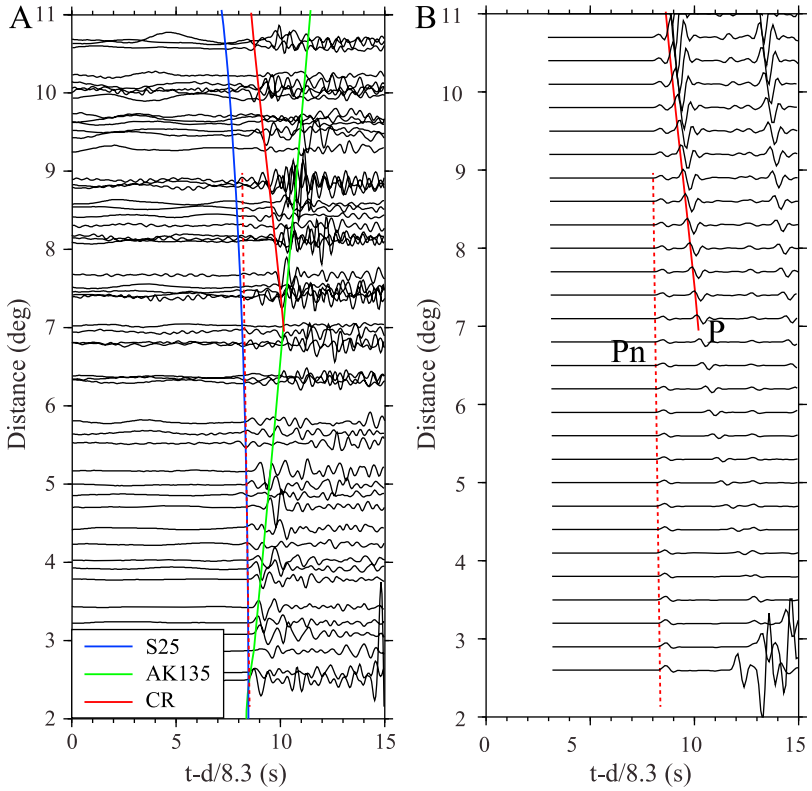

Figure 11. Record section for the Oklahoma earthquake is plotted with a reduce velocity of 8.3 km/s. (a) The travel-time predictions for the three models are displayed with color lines, S25 (blue), AK135 (green), and CR (red). Note that AK135 does not have a LAB and has a continuous travel time curve. Dotted lines denote P_n while the solid lines indicate the P arrivals. (b) The synthetic waveforms generated from the CR model are displayed. The data and synthetics are scaled in the true amplitude multiplied by the epicentral distance in km. The model CR predicts the low amplitude and velocity change at 8° quite well.

this feature is consistent at all azimuths so we consider a robust regional feature (Figure S7).

[18] Upper mantle arrivals with turning depths near the 410 discontinuity exhibit significant differences between northern and southern TA stations (Figure 10). We divide the data along an azimuth indicated in Figure 2. We present a comparison of northern (I) and southern (II) waveforms for the distance from 18° to 20.5°. The comparison highlights differences in shape of the CD pulse near 19.5° where the northern stations are broadened and poorly fit by the CR synthetics compared to the southern profile. Broadened CD branches can be caused by late arrival of BC branch, which is reflected from the 410 discontinuity and usually has small amplitude and similar arrival time as CD. We examine all waveforms at this distance range and map the anomalous stations and their turning points in Figure 10b along with timing difference between BC and CD. It becomes difficult to separate these two arrivals by injecting anomalous velocities above 300 km since the raypaths sample the same region at shallower depths. Thus, structural changes just above or below the 410 prove the most effective. A possible explanation is inserting a box of slow velocities, reduced by ~3% with a thickness of 20 km and a width of about 100 km (Figures 10c and 10d). Similar features have been found to explain triplication data in the western U.S. as discussed by *Song and Helmberger* [2006]. We acknowledge that a well-placed anomaly at slightly shallower depth could also cause such features. In short, we can explain the main features of the observed upper mantle triplications with the 1-D CR model quite well, but there is evidence for interesting small-scale deviations from the 1-D structure.

5. Uppermost Mantle Constraints

[19] The velocity structure below 200 km appears to be well approximated by a 1-D model, but stronger lateral variations are expected in the upper 200 km. We seek to obtain high-resolution estimates of the radial P velocity structure of the continental lithosphere, allowing for small timing shifts

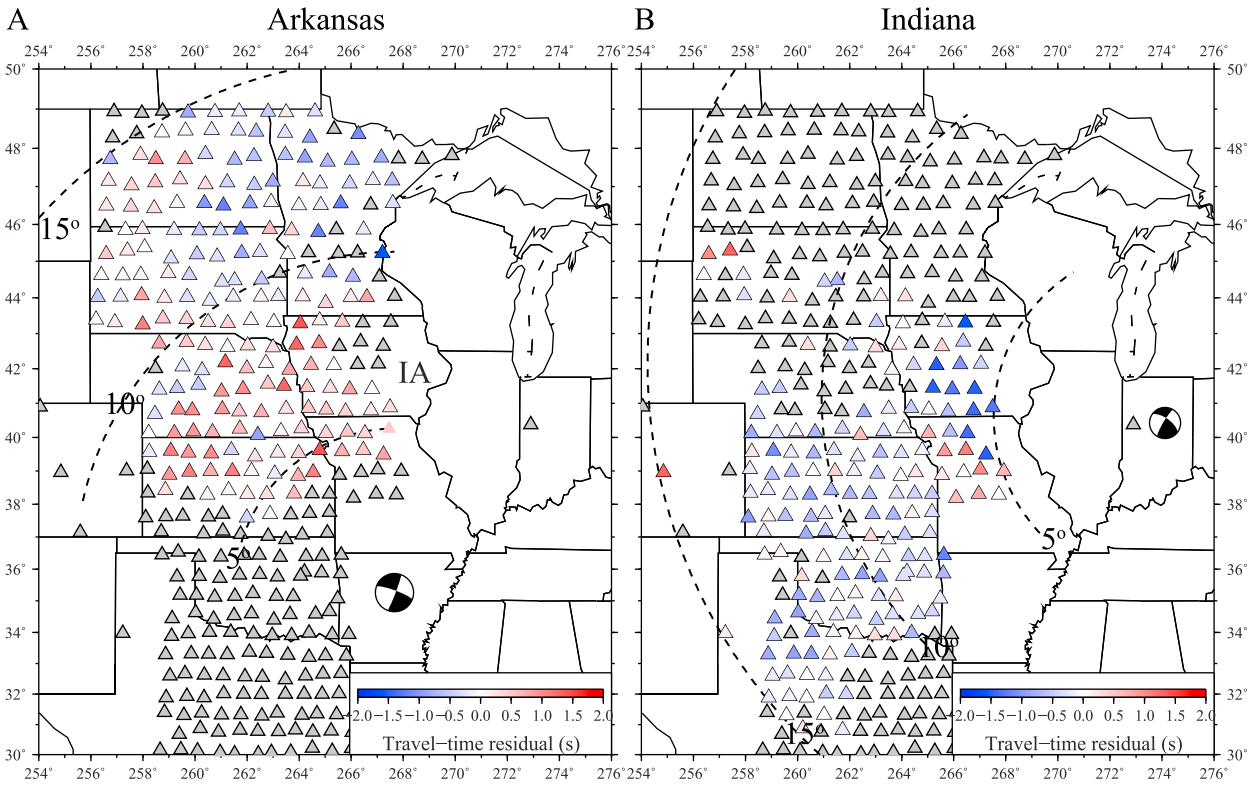

Figure 12. Travel-time residuals for (a) the Arkansas earthquake and (b) the Indiana earthquake. The distances are indicated with dotted arcs, starting at 5°. IA: Iowa.

to account for lateral variations. Analysis of the first arrival transition from P_n to P provides sensitivity to the radial P velocity gradient in the lithosphere and thickness of the lithosphere that cannot be achieved by other methods such as receiver functions or surface wave dispersion [e.g., *Eaton et al.*, 2009]. Here, we display a few record sections that confirm earlier studies reporting an 8° discontinuity in first arrivals [*Thybo and Perchuć*, 1997].

[20] We first take advantage of the TA stations and the Oklahoma earthquake (Figure 2). The data and synthetics are scaled in absolute amplitude multiplied by the distance (Figure 11). Amplitude decay with increasing distance is much less than observed in western data sets [*Romney et al.*, 1962]. Additionally, the waveforms are not coherent from station-to-station, which is common at this distance range and has been previously modeled with alternating fast-slow fine-scale layering [*Perchuć and Thybo*, 1996]. We do not attempt to model this feature and instead concentrate on the shadow zone where P_n decays and the deeper sampling P emerges near 8–9°, consistent with *Thybo and Perchuć* [1997]. Timing lines predicted by S25, CR, and AK135 illuminate the substantial differences between predicted arrival times. Note that AK135 travel times are over 5.0 s late at the larger ranges. Since the event is well located and the profile is completely covered with stations (Figure 11a), the absolute velocities are unusually well constrained. Modeling P_n waveforms at longer periods is possible as demonstrated by *Chu et al.* [2012], but because the magnitude of this event is small, periods greater than about 2 s are found to have poor signal-to-noise.

[21] In Figure 12, we present the station distribution for two other events, one in Arkansas and one in Indiana, to the east of the Oklahoma earthquake. These events are strike-slip earthquakes with the mechanisms given in Table 1. Individual observations are cross-correlated with synthetics from CR and shifted for best alignment, the same processing we use for the Quebec earthquake. These shifts are mapped in Figure 12. The largest shifts are >1 s and in general the timing shifts indicate significant lateral variations in structure. Moreover, the smoothness of timing shifts over length-scales of a few hundred km suggests they are predominantly associated with variations in the lithospheric mantle rather than variations in upper crustal structure. The record sections in Figure 13 are chosen for an azimuth corridor with strong P wave radiation and stacked with normalized amplitudes. When stacked

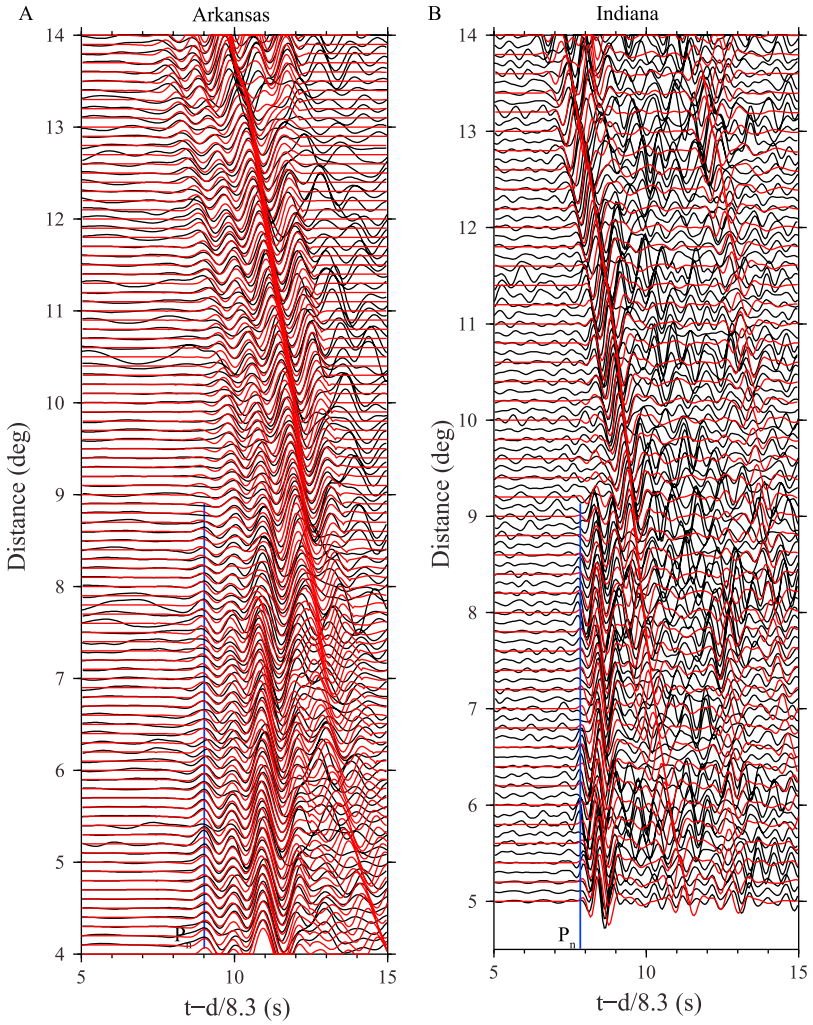

Figure 13. Comparison of vertical *P* displacement (black) and synthetics (red) for (a) the Arkansas earthquake and (b) the Indiana earthquake. The data are stacked using a bin size of 0.1° and aligned using the travel-time residuals shown in Figure 12. The Arkansas earthquake is filtered at 0.3–2.0 Hz, while the Indiana earthquake is filtered at 0.8–2.0 Hz. Blue lines denote arrival time of P_n waves.

along an azimuth corridor, the waveform patterns are remarkably coherent and the degree of consistency between observed and CR synthetic waveforms at high frequencies (up to 2 Hz) is impressive. These record sections are plotted relative to the nearest stations along these profiles. The Indiana event (12 km) is deeper than the Arkansas event (4 km) (Table 1), thus the P_n phase arrives earlier for the former event by over a second. Note that the 1.5 s backward jump in arrival time of the Indiana event at the ∼9° change from P_n to P cannot be caused by strong lateral variations as this would be apparent in the travel-time shifts shown in Figure 12. The record sections with and without corrections are shown in Figure S8 and the change in travel time slope is easily observed near ∼8–9°. The backward jump in arrival time at the change from P_n to P is more pronounced for the Indiana event on account of its deeper hypocenter (which separates the direct and surface-reflected arrivals) and higher frequency filtering (0.8–2 Hz for the Indiana event, 0.3–2 Hz for the Arkansas event). This abrupt transition results from a 1% velocity jump at 120 km in CR, which separates a slight negative velocity gradient in the shallower portion of the lid from a positive gradient in the deeper part of the lid.

6. Discussion

[22] Constraints on the 3-D velocity structure of eastern North America are bound to increase because the TA has just now crossed the Mississippi River

at the time of this reporting. Nevertheless, by modeling these events just beyond the array, we have established a useful upper mantle reference model for future seismic studies and for consideration of the properties and history of the tectosphere beneath a portion of the interior of North America. Knowledge of the basal structure of North America and mantle transition zone structure beneath the continental interior has become increasingly important in light of evidence that flat subduction beneath the continental lithosphere during the Cretaceous [*Coney and Reynolds*, 1977] probably extended as far inboard as the western edge of the Great Lakes [*Liu et al.*, 2008; *Spasojevic et al.*, 2009]. The basic idea is that the pattern of subsidence created by emplacement of the cold slab beneath the continent is fundamentally linked to the distribution of sedimentation in Cretaceous interior sea [*Smith et al.*, 1994]. A suggested trigger for the slab flattening event is ∼90 Ma subduction of a thick buoyant oceanic plateau beneath the southwestern U.S. margin [*Livaccari et al.*, 1981; *Saleeby*, 2003; *Liu et al.*, 2010]. The interior sea disappeared about 60 Ma and dynamic modeling predicts the slab fell away from the base of North America at about this time and began to sink into the lower mantle with an east-dipping trajectory [*Liu et al.*, 2010; *Spasojevic et al.*, 2009]. The question is, can we find any evidence for this hypothesis in high-resolution seismology other than the present deep tomographic images [e.g., *Grand*, 2002; *Sigloch*, 2011]?

[23] Our modeling produces a relatively simple 1-D structure without much evidence for deep lateral heterogeneity. However, there appear to be anomalous features of phase transition boundaries that may be indicative of slab history. In Figure 14, we display a cross-section through the tomographic model along with some of our results [*Grand*, 2002]. This tomographic image was generated from a mixture of modern digital data and older analog seismograms used in constructing SNA and TNA (see Figure 1). The reference model is the average of the two regional models and the top 300 km is heavily saturated so that the lower structure can be observed. The tomography model shows only small±0.4% variations in the transition zone. On the left, the craton structure transitions into TNA that appears to be overly simplified in *Grand*'s [2002] model. The multipathing results presented by *Sun and Helmberger* [2011] indicates a strongly heterogeneous structure extending eastward beyond the Black Hills with a sharp horseshoe-shaped boundary extending beneath Nebraska (Figure 14b). This slow feature is also apparent in travel time delays from the CR modeling experiment and extended further in Figure 12a beneath Iowa. This corridor is discussed by *Liu et al.* [2010] as the path of a sinking hypothetical thickened slab and still appears anomalous where perhaps warmer upwelling material has replaced the cold slab.

[24] The anomalous zone above the 410 discontinuity is near the expected region of slab penetration and occurs at the western edge of a mild slow region in the tomography, i.e., location 9, beneath Wisconsin (Figure 14b). A low-velocity anomaly could represent partial melt created by upward return flow across the 410 if the transition zone is sufficiently hydrated [e.g., *Bercovici and Karato*, 2003]. However, our inference of a low-velocity anomaly above the 410 is a non-unique explanation for the late arrival of the BC branch so interpretations regarding the origin of such an anomaly are speculative. The expected disturbance of this discontinuity is difficult to interpret because of the uncertainties in the presence of water versus temperature as recently discussed by *Cao and Levander* [2010]. They find a 25 km upward shift of the 410 beneath Nevada and a 35 km downward shift of the 660 beneath Utah that are spatially correlated with high-velocity slabs [*Sigloch et al.*, 2008]. They also observe a double 660 discontinuity associated with the subducting Gorda slab, as found in this study, at the eastern edge of this structure (see their Figure 13). These features are compatible with many tomographic models and waveform analysis [*Chu et al.*, 2012]. In short, there appears to be some seismic evidence for such a slab passageway along this corridor. This report concentrated on mostly horizontal paths while tomographic models address mostly vertical paths. Combining these two approaches should greatly improve resolution and will be attempted with the completion of the TA experiment.

[25] *P* waveforms from the small events consistently indicate a changeover from P_n to *P* near 8°. These events sample the same region where *Green and Hales* [1968] first noted this discontinuity from refraction profiles produced by the Early Rise experiment (explosions in Lake Superior). The apparent discontinuity, which has recently been called the mid-lithospheric discontinuity (MLD), is observed in many different types of data as discussed by *Abt et al.* [2010]. The original explanation of MLD is that it is a phase change from spinel to garnet, but *Stixrude and Lithgow-Bertelloni* [2005] dispute this conclusion. *Thybo* [2006] argues for a small percentage of melt caused by the presence of carbon or water. More recently,

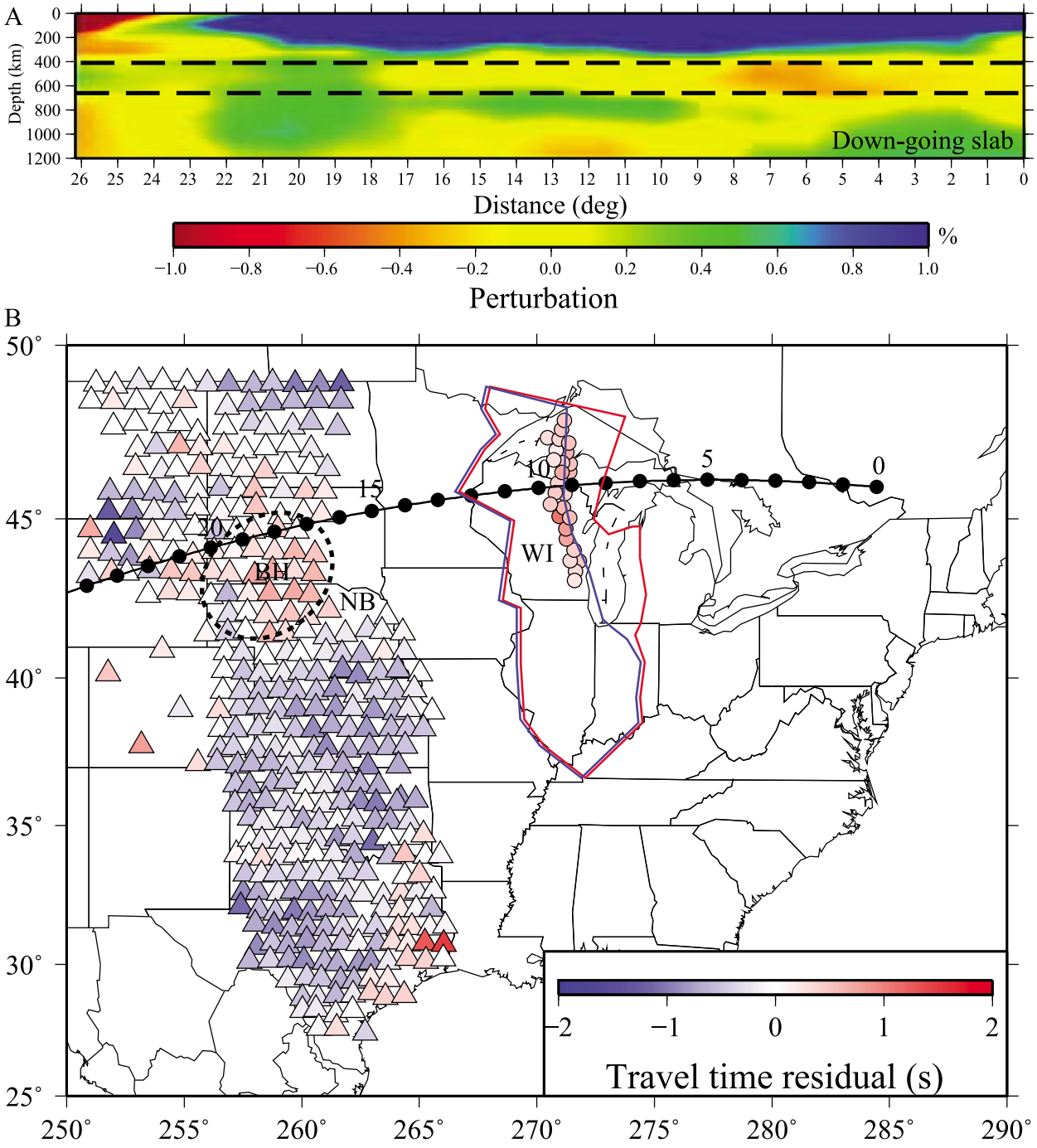

Figure 14. (a) *S* velocity perturbation from *Grand* [2002] along the path from the Quebec earthquake to the Black Hills showing the possible downgoing Farallon slab and the relatively high velocity near the 660 discontinuity near position 4. (b) The location of the profile is shown. In Figure 14b, bid-points of the CD branch (red) and EF branch (blue) for TA are enclosed by the polygons. The travel-time residuals (triangles) and anomalous CD branch (colored circles) are displayed. Black dots are epicentral distance with intervals of 1°. Dashed oval denotes the Black Hills anomaly. BH: Black Hills; NB: Nebraska; WI: Wisconsin.

Yuan and Romanowicz [2010] interpret the MLD as a sudden change in anisotropy. *Van der Lee et al.* [2008] suggest that the Farallon slab has provided the volatiles to generate such zones of weakness. A number of new events have occurred in the last few months and display more evidence for lateral variation [*Chu and Helmberger*, 2011]. Perhaps, with a larger data set of regional events a clearer

picture of lateral variations in lithospheric structure will emerge.

[26] We have modeled waveforms from four earthquake sources in the interior of North America to determine a suitable reference model and identify isolated areas that are inconsistent with purely 1-D structure. The strongest event was used to conduct a grid-search analysis of the major upper mantle discontinuities. Our results are similar to earlier models, such as SNA, except we find the 660 boundary better explained by two smaller velocity jumps 16 km apart rather than a single larger velocity jump. Additionally we find that a compact low-velocity anomaly may exist just above the 410 beneath Wisconsin. The relationship, if any, between these structures and subduction history will become clearer as the TA proceeds eastward. Small earthquakes were used to investigate the lithospheric structure, and our results support earlier reports on the existence of the 8° discontinuity caused by a low-velocity zone from 40 to 120 km followed by a significant jump of 1% and positive gradient down to 165 km.

Acknowledgments

[27] We would like to thank Thorsten Becker, the associated editor, and two anonymous reviewers. Their suggestions and comments made significant improvements to the manuscript. Seismic data in this study was obtained from IRIS data management center. This work was supported by National Science Foundation through grant EAR-0639507 and the Caltech Tectonic Observatory. Contribution number 10071 of the Seismological Laboratory, California Institute of Technology.

References

Abt, D. L., K. M. Fischer, S. W. French, H. A. Ford, H. Yuan, and B. Romanowicz (2010), North American lithospheric discontinuity structure imaged by *Ps* and *Sp* receiver functions, *J. Geophys. Res.*, *115*, B09301, doi:10.1029/2009JB006914.

Ai, Y., T. Zheng, W. Xu, Y. He, and D. Dong (2003), A complex 660 km discontinuity beneath northeast China, *Earth Planet. Sci. Lett.*, *212*, 63–71, doi:10.1016/S0012-821X(03)00266-8.

Bercovici, D., and S. Karato (2003), Whole mantle convection and the transition zone water filter, *Nature*, *425*, 39–44, doi:10.1038/nature01918.

Bird, P. (1979), Continental delamination and the Colorado Plateau, *J. Geophys. Res.*, *84*(B13), 7561–7571.

Burdick, S., R. D. van der Hilst, F. L. Vernon, V. Martynov, T. Cox, J. Eakins, T. Mulder, L. Astiz, and G. L. Pavlis (2009), Model update December 2008: Upper mantle heterogeneity beneath North America from *P* wave travel time tomography with global and USArray Transportable Array data, *Seismol. Res. Lett.*, *80*(4), 638–645, doi:10.1785/gssrl.80.4.638.

Cao, A., and A. Levander (2010), High-resolution transition zone structures of the Gorda Slab beneath the western United States: Implication for deep water subduction, *J. Geophys. Res.*, *115*, B07301, doi:10.1029/2009JB006876.

Carlson, R. W., and A. J. Irving (1994), Depletion and enrichment history of subcontinental lithospheric mantle: An Os, Sr, Nd and Pb isotopic study of ultramafic xenoliths from the northwestern Wyoming Craton, *Earth Planet. Sci. Lett.*, *126*, 457–472, doi:10.1016/0012-821X(94)90124-4.

Carlson, R. W., D. G. Pearson, and D. E. James (2005), Physical, chemical, and chronological characteristics of continental mantle, *Rev. Geophys.*, *43*, RG1001, doi:10.1029/2004RG000156.

Chu, R., and D. V. Helmberger (2011), Upper-mantle *P*-velocity structure beneath the Eastern United States: Superficially simple but deeply diverse, paper presented at the Institute on the Lithosphere Asthenosphere Boundary, EarthScope LAB Inst., Portland, Oreg., 19–21, Sept.

Chu, R., B. Schmandt, and D. V. Helmberger (2012), Juan de Fuca subduction zone from a mixture of tomography and waveform modeling, *J. Geophys. Res.*, doi:10.1029/2012JB009146, in press.

Coney, P. J., and S. J. Reynolds (1977), Flattening of the Farallon slab, *Nature*, *270*, 403–406, doi:10.1038/270403a0.

Courtier, A. M., and J. Revenaugh (2006), A water-rich transition zone beneath the eastern United States and Gulf of Mexico from multiple *ScS* reverberations, in *Earth's Deep Water Cycle*, *Geophys. Monogr. Ser.*, vol. 168, edited by S. D. Jacobsen and S. van der Lee, pp. 181–193, AGU, Washington, D. C., doi:10.1029/168GM14.

Deuss, A., S. Redfern, K. Chambers, and J. Woodhouse (2006), The nature of the 660 kilometer discontinuity in Earth's mantle from global observations of *PP* precursors, *Science*, *311*, 198–201, doi:10.1126/science.1120020.

Dziewonski, A. M., and D. L. Anderson (1981), Preliminary reference Earth model, *Phys. Earth Planet. Inter.*, *25*, 297–356, doi:10.1016/0031-9201(81)90046-7.

Eagar, K. C., M. J. Fouch, and D. E. James (2010), Receiver function imaging of upper mantle complexity beneath the Pacific Northwest, United States, *Earth Planet. Sci. Lett.*, *297*, 141–153, doi:10.1016/j.epsl.2010.06.015.

Eaton, D. W., F. Darbyshire, R. L. Evans, H. Grütter, A. G. Jones, and X. Yuan (2009), The elusive lithosphere-asthenosphere boundary (LAB) beneath cratons, *Lithos*, *109*, 1–22, doi:10.1016/j.lithos.2008.05.009.

Ekström, G., and A. M. Dziewonski (1998), The unique anisotropy of the Pacific upper mantle, *Nature*, *394*, 168–172, doi:10.1038/28148.

Engebretsen, D. C., A. Cox, and R. G. Gordon (1985), Relative motions between oceanic and continental plates in the Pacific Basin, *Spec. Pap. Geol. Soc. Am.*, *206*, 560–569.

Faul, U. H., and I. Jackson (2005), The seismological signature of temperature and grain size variations in the upper mantle, *Earth Planet. Sci. Lett.*, *234*(1–2), 119–134, doi:10.1016/j.epsl.2005.02.008.

Fischer, K. M., H. A. Ford, D. L. Abt, and C. A. Rychert (2010), The lithosphere-asthenosphere boundary, *Annu. Rev. Earth Planet. Sci.*, *38*(5), 51–75.

Gaherty, J. B., T. H. Jordan, and L. S. Gee (1996), Seismic structure of the upper mantle in a central Pacific corridor, *J. Geophys. Res.*, *101*(B10), 22,291–22,309, doi:10.1029/96JB01882.

Gaherty, J. B., M. Kato, and T. H. Jordan (1999), Seismological structure of the upper mantle: A regional comparison of seismic layering, *Phys. Earth Planet. Inter.*, *110*, 21–41, doi:10.1016/S0031-9201(98)00132-0.

Gao, S., R. L. Rudnick, R. W. Carlson, W. F. McDonough, and Y. Liu (2002), Re-Os evidence for replacement of ancient mantle lithosphere beneath the North China Craton, *Earth Planet. Sci. Lett.*, *198*, 307–322, doi:10.1016/S0012-821X(02)00489-2.

Gao, W., E. Matzel, and S. P. Grand (2006), Upper mantle seismic structure beneath eastern Mexico determined from *P* and *S* waveform inversion and its implications, *J. Geophys. Res.*, *111*, B08307, doi:10.1029/2006JB004304.

Given, J. W., and D. V. Helmberger (1980), Upper mantle structure of Northwestern Eurasia, *J. Geophys. Res.*, *85*, 7183–7194, doi:10.1029/JB085iB12p07183.

Godey, S., F. Deschamps, J. Trampert, and R. Snieder (2004), Thermal and compositional anomalies beneath the North American continent, *J. Geophys. Res.*, *109*, B01308, doi:10.1029/2002JB002263.

Grand, S. P. (2002), Mantle shear-wave tomography and the fate of subducted slabs, *Philos. Trans. R. Soc. London, Ser. A*, *360*, 2475–2491, doi:10.1098/rsta.2002.1077.

Grand, S. P., and D. V. Helmberger (1984), Upper mantle shear structure of North America, *Geophys. J. R. Astron. Soc.*, *76*, 399–438.

Green, D. H., and A. L. Hales (1968), The travel times of *P* waves to 30° in the central United States and upper mantle structure, *Bull. Seismol. Soc. Am.*, *58*, 267–289.

Herrmann, R. B. (1979), Surface wave focal mechanisms for eastern North American earthquakes with tectonic implications, *J. Geophys. Res.*, *84*(B7), 3543–3552, doi:10.1029/JB084iB07p03543.

Herrmann, R. B., H. Benz, and C. J. Ammon (2011), Monitoring the earthquake source process in North America, *Bull. Seismol. Soc. Am.*, *101*(6), 2609–2625, doi:10.1785/0120110095.

Jasbinsek, J., and K. G. Dueker (2007), Ubiquitous low-velocity layer atop the 410 km discontinuity in the northern Rocky Mountains, *Geochem. Geophys. Geosyst.*, *8*, Q10004, doi:10.1029/2007GC001661.

Jordan, T. H. (1978), Composition and development of the continental tectosphere, *Nature*, *274*, 544–548, doi:10.1038/274544a0.

Karato, S.-I., and P. Wu (1993), Rheology of the upper mantle: A synthesis, *Science*, *260*, 771–778, doi:10.1126/science.260.5109.771.

Kennett, B., E. R. Engdahl, and R. Buland (1995), Constraints on seismic velocity in the Earth from travel times, *Geophys. J. Int.*, *122*, 108–124, doi:10.1111/j.1365-246X.1995.tb03540.x.

Lee, C. T. A., P. Luffi, and E. J. Chin (2011), Building and destroying continental mantle, *Annu. Rev. Earth Planet. Sci.*, *39*, 59–90, doi:10.1146/annurev-earth-040610-133505.

LeFevre, L. V., and D. V. Helmberger (1989), Upper mantle *P* velocity structure of the Canadian Shield, *J. Geophys. Res.*, *94*(B12), 17,749–17,765, doi:10.1029/JB094iB12p17749.

Levander, A., B. Schmandt, M. S. Miller, K. Liu, K. E. Karlstrom, R. S. Crow, C.-T. A. Lee, and E. D. Humphreys (2011), Continuing Colorado plateau uplift by delamination-style convective lithospheric downwelling, *Nature*, *472*, 461–465, doi:10.1038/nature10001.

Li, A., K. M. Fischer, M. E. Wysession, and T. J. Clarke (1998), Mantle discontinuities and temperature under the North American continental keel, *Nature*, *395*, 160–163, doi:10.1038/25972.

Liu, L., S. Spasojević, and M. Gurnis (2008), Reconstructing Farallon Plate subduction beneath North America back to the late Cretaceous, *Science*, *322*, 934–938, doi:10.1126/science.1162921.

Liu, L., M. Gurnis, M. Seton, J. Saleeby, R. D. Müller, and J. Jackson (2010), The role of oceanic plateau subduction in the Laramide Orogeny, *Nat. Geosci.*, *3*, 353–357, doi:10.1038/ngeo829.

Livaccari, R. F., K. Burke, and A. M. C. Sengor (1981), Was the Laramide orogeny related to subduction of an oceanic plateau, *Nature*, *289*, 276–278, doi:10.1038/289276a0.

Ma, S., and D. W. Eaton (2011), Combining double-difference relocation with regional depth-phase modeling to improve hypocenter accuracy, *Geophys. J. Int.*, *185*, 871–889, doi:10.1111/j.1365-246X.2011.04972.x.

Matzel, E., and S. P. Grand (2004), The anisotropic seismic structure of the East European platform, *J. Geophys. Res.*, *109*, B01302, doi:10.1029/2001JB000623.

Mereu, R. F., and J. A. Hunter (1969), Crustal and upper mantle structure under the Canadian Shield from Project Early Rise data, *Bull. Seismol. Soc. Am.*, *59*(1), 147–165.

Moschetti, M. P., M. H. Ritzwoller, F.-C. Lin, and Y. Yang (2010), Crustal shear wave velocity structure of the western United States inferred from ambient seismic noise and earthquake data, *J. Geophys. Res.*, *115*, B10306, doi:10.1029/2010JB007448.

Nettles, M., and A. M. Dziewonski (2008), Radially anisotropic shear velocity structure of the upper mantle globally and beneath North America, *J. Geophys. Res.*, *113*, B02303, doi:10.1029/2006JB004819.

Obrebski, M., R. M. Allen, M. Xue, and S. Hung (2010), Slab plume interaction beneath the Pacific Northwest, *Geophys. Res. Lett.*, *37*, L14305, doi:10.1029/2010GL043489.

Perchuć, E., and H. Thybo (1996), A new model of upper mantle *P* wave velocity below the Baltic Shield: Indication of partial melt in the 95 to 160 km depth range, *Tectonophysics*, *253*, 227–245, doi:10.1016/0040-1951(95)00057-7.

Pollitz, F. F., and J. A. Snoke (2010), Rayleigh-wave phase-velocity maps and three-dimensional shear velocity structure of the western US from local non-plane surface wave tomography, *Geophys. J. Int.*, *180*, 1153–1169, doi:10.1111/j.1365-246X.2009.04441.x.

Ringwood, A. E. (1975), *Composition and Petrology of the Earth's Mantle*, 618 pp., McGraw Hill, New York.

Romney, C., B. G. Brooks, R. H. Mansfield, D. S. Carder, J. N. Jordan, and D. W. Gordon (1962), Travel times and amplitudes of principal body phases recorded from Gnome, *Bull. Seismol. Soc. Am.*, *52*, 1057–1074.

Roth, J. B., M. J. Fouch, D. E. James, and R. W. Carlson (2008), Three-dimensional seismic velocity structure of the northwestern United States, *Geophys. Res. Lett.*, *35*, L15304, doi:10.1029/2008GL034669.

Saleeby, J. (2003), Segmentation of the Laramide slab-evidence from the southern Sierra Nevada region, *Geol. Soc. Am. Bull.*, *115*, 655–668, doi:10.1130/0016-7606(2003)115<0655:SOTLSF>2.0.CO;2.

Schaeffer, A. J., and M. G. Bostock (2010), A low-velocity zone atop the transition zone in northwestern Canada, *J. Geophys. Res.*, *115*, B06302, doi:10.1029/2009JB006856.

Schmandt, B., and E. Humphreys (2010), Complex subduction and small-scale convection revealed by body-wave tomography of the western United States upper mantle, *Earth Planet. Sci. Lett.*, *297*, 435–445, doi:10.1016/j.epsl.2010.06.047.

Schmandt, B., K. G. Dueker, S. M. Hansen, J. J. Jasbinsek, and Z. Zhang (2011), A sporadic low-velocity layer atop the western U.S. mantle transition zone and short-wavelength variations in transition zone discontinuities, *Geochem. Geophys. Geosyst.*, *12*, Q08014, doi:10.1029/2011GC003668.

Sigloch, K. (2011), Mantle provinces under North America from multifrequency *P* wave tomography, *Geochem. Geophys. Geosyst.*, *12*, Q02W08, doi:10.1029/2010GC003421.

Sigloch, K., N. McQuarrie, and G. Nolet (2008), Two-stage subduction history under North America inferred from multiple-frequency tomography, *Nat. Geosci.*, *1*, 458–462, doi:10.1038/ngeo231.

Simmons, N. A., and H. Gurrola (2000), Multiple seismic discontinuities near the base of the transition zone in the Earth's mantle, *Nature*, *405*, 559–562, doi:10.1038/35014589.

Smith, A. G., D. G. Smith, and B. M. Funnel (1994), *Atlas of Mesozoic and Cenozoic Coastlines*, 99 pp., Cambridge Univ. Press, New York.

Song, T. A., and D. V. Helmberger (2006), Low velocity zone atop the transition zone in the western US from *S* waveform triplication, in *Earth's Deep Water Cycle*, *Geophys. Monogr. Ser.*, vol. 168, edited by S. D. Jacobsen and S. van der Lee, pp. 195–213, AGU, Washington, D. C., doi:10.1029/168GM15.

Song, T. R. A., and D. V. Helmberger (2007), A depleted, destabilized continental lithosphere near the Rio Grande rift, *Earth Planet. Sci. Lett.*, *262*, 175–184, doi:10.1016/j.epsl.2007.07.052.

Spasojevic, S., L. Liu, and M. Gurnis (2009), Adjoint models of mantle convection with seismic, plate motion, and stratigraphic constraints: North America since the Late Cretaceous, *Geochem. Geophys. Geosyst.*, *10*, Q05W02, doi:10.1029/2008GC002345.

Stixrude, L., and C. Lithgow-Bertelloni (2005), Mineralogy and elasticity of the oceanic upper mantle: Origin of the low-velocity zone, *J. Geophys. Res.*, *110*, B03204, doi:10.1029/2004JB002965.

Sun, D., and D. V. Helmberger (2011), Upper mantle structures beneath USArray derived from waveform complexity, *Geophys. J. Int.*, *184*(1), 416–438, doi:10.1111/j.1365-246X.2010.04847.x.

Tan, Y., and D. V. Helmberger (2007), Trans-Pacific upper mantle shear velocity structure, *J. Geophys. Res.*, *112*, B08301, doi:10.1029/2006JB004853.

Tan, Y., A. Song, S. Wei, and D. Helmberger (2010), Surface wave path corrections and source inversions in southern California, *Bull. Seismol. Soc. Am.*, *100*, 2891–2904, doi:10.1785/0120090063.

Tauzin, B., E. Debayle, and G. Wittlinger (2010), Seismic evidence for a global low velocity layer in the Earth's upper mantle, *Nat. Geosci.*, *3*, 718–721, doi:10.1038/ngeo969.

Thybo, H. (2006), The heterogeneous upper mantle low velocity zone, *Tectonophysics*, *416*, 53–79, doi:10.1016/j.tecto.2005.11.021.

Thybo, H., and E. Perchuć (1997), The seismic 8° discontinuity and partial melting in continental mantle, *Science*, *275*, 1626–1629, doi:10.1126/science.275.5306.1626.

Vacher, P., A. Mocquet, and C. Sotin (1998), Computation of seismic profiles from mineral physics: The importance of the non-olivine components for explaining the 660 km depth discontinuity, *Phys. Earth Planet. Inter.*, *106*, 275–298, doi:10.1016/S0031-9201(98)00076-4.

van der Lee, S., K. Regenauer-Lieb, and D. A. Yuen (2008), The role of water in connecting past and future episodes of subduction, *Earth Planet. Sci. Lett.*, *273*, 15–27, doi:10.1016/j.epsl.2008.04.041.

Yuan, H., and B. Romanowicz (2010), Lithospheric layering in the North American continent, *Nature*, *466*, 1063–1068, doi:10.1038/nature09332.

Zhang, S., and S.-I. Karato (1995), Lattice preferred orientation of olivine aggregates deformed in simple shear, *Nature*, *375*, 774–777, doi:10.1038/375774a0.

Zhu, L., and D. V. Helmberger (1996), Advancement in source estimation techniques using broadband regional seismograms, *Bull. Seismol. Soc. Am.*, *86*, 1634–1641.